Effective Hydrogenation of Poly-Si Passivating Contacts by Atomic-Layer-Deposited Nickel Oxide

Nga Phung, Cristian van Helvoirt, Wolfhard Beyer, John Anker, Ronald C. G. Naber, Marten Renes, Wilhelmus M. M. Kessels, L. J. Geerligs, Mariadriana Creatore, and Bart Macco

***Abstract*—In recent years, passivating contacts based on SiO_2/poly-Si have proven to be an enabling technology for Si solar cells. Effective hydrogenation of the interfacial SiO_2 is vital for realizing efficient contacts. Hydrogen-rich dielectrics, such as SiN_x and Al_2O_3, are commonly employed for hydrogenation, whereas also recently, *n*-type conductive oxides, such as In_2O_3:Sn and ZnO, have been demonstrated to yield excellent hydrogenation. This study presents the use of a *p*-type metal oxide, specifically NiO, as a suitable hydrogenation source. The *p*-type character of NiO makes it an interesting candidate for hydrogenation because of its potential use in selective contacting structures. Herein, we show that NiO, synthesized by atomic layer deposition (ALD), can be used to hydrogenate poly-Si/SiO_2 contacts effectively. Furthermore, we benchmark its hydrogenation performance to the established ALD ZnO/Al_2O_3 stack and provide insights into the hydrogenation process. On planar surfaces, NiO yields almost as excellent results as ZnO/Al_2O_3 stacks, whereas it lags behind on more challenging textured surfaces. Interestingly, even though elastic recoil detection analysis reveals that ALD NiO is rich in hydrogen, secondary ion mass spectrometry measurements show that, when NiO is compared to the ZnO/Al_2O_3 stack, less hydrogen is present at the Si/SiO_2 interface after annealing. This is explained from effusion measurements, which show substantial effusion of hydrogen from NiO around 300 °C. Hence, Al_2O_3 capping is further employed to prevent hydrogen loss and on textured wafers, the NiO/Al_2O_3 stacks on poly-Si achieve an implied open-circuit voltage of 728 mV, confirming the excellent hydrogenation from ALD metal oxides.**

***Index Terms*—Hydrogenation, nickel oxide, passivating contact, silicon solar cells, surface passivation.**

Manuscript received 5 April 2022; revised 23 August 2022; accepted 9 September 2022. Date of publication 28 September 2022; date of current version 28 November 2022. This work was supported by the Top Consortia for Knowledge and Innovation Solar Energy Program "PERCspective" (TEUE119005) of the Ministry of Economic Affairs of The Netherlands. *(Corresponding author: Bart Macco.)*

Nga Phung, Cristian van Helvoirt, Wilhelmus M. M. Kessels, Mariadriana Creatore, and Bart Macco are with the Department of Applied Physics, Eindhoven University of Technology, 5612 AZ Eindhoven, The Netherlands (e-mail: t.t.n.phung@tue.nl; c.v.helvoirt@tue.nl; w.m.m.kessels@tue.nl; m.creatore@tue.nl; b.macco@tue.nl).

Wolfhard Beyer is with the IEK5-Photovoltaik, Forschungszentrum Jülich, 52428 Jülich, Germany (e-mail: w.beyer@fz-juelich.de).

John Anker and L. J. Geerligs are with the TNO, 1755 LE Petten, The Netherlands (e-mail: john.anker@tno.nl; bart.geerligs@tno.nl).

Ronald C. G. Naber was with the Tempress Systems BV, 8171 MD Vaassen, The Netherlands. He is now with the Semco Smartech, 34160 Castries, France (e-mail: rcgnaber@gmail.com).

Marten Renes is with the Tempress Systems BV, 8171 MD Vaassen, The Netherlands (e-mail: mrenes@tempress.nl).

Color versions of one or more figures in this article are available at https://doi.org/10.1109/JPHOTOV.2022.3206895.

Digital Object Identifier 10.1109/JPHOTOV.2022.3206895

I. Introduction

One of the key developments in silicon solar cell technology consists of the improvement of the absorber surface passivation quality and development of charge carrier-selective layers [1], [2], [3], [4], [5]. Serving both as a selective contact and surface passivation layer, doped poly-Si with an ultrathin SiO_2 tunneling oxide has been adopted increasingly in silicon photovoltaics (PV). The poly-Si passivating contact enables highly efficient devices, so called TOPCon and POLO structures, achieving more than 26% due to excellent charge selectivity and well-passivated silicon surfaces [6], [7], [8]. This structure enables commercialized TOPCon PV modules with efficiencies in excess of 23% [9]. It has been proposed that the surface passivation originates from field-effect passivation (also referred to as carrier population control [3]) by the doped poly-Si layer. Due to the degenerate doping of poly-Si, it induces a strong band bending at the SiO_2/c-Si(*n*) interface reducing the surface recombination as can be seen in Fig. 1. A higher doping level of poly-Si is expected to have higher field-effect passivation level and better surface passivation.

In addition to field-effect passivation, the surface passivation of poly-Si/SiO_2 passivating contact is due to chemical passivation at the interfacial SiO_2. Hydrogen plays a key role in chemical passivation of the interfacial oxide by binding to defects. However, during high temperature processing of poly-Si (700–900 °C), hydrogen effuses from the structure, reducing the passivation quality [10]. Hence, it is desirable to resupply hydrogen after the formation of doped poly-Si for an effective chemical passivation, as also shown schematically in Fig. 1. This hydrogenation step can be done by hydrogen plasma treatment or by employing H-rich dielectric materials, such as SiN_x and Al_2O_3 [11], [12], as well as hydrogenated transparent conductive oxides, such as indium tin oxide (ITO) and Al-doped ZnO [4], [13].

Among the fabrication methods for depositing hydrogenated metal oxides, atomic layer deposition (ALD) has been used widely for silicon surface passivation, mainly thanks to the ability to make ultrathin layers with a high material quality [14], [15], [16], [17]. In fact, various ALD metal oxides have proven to give excellent hydrogenation quality. Previous reports have shown that ALD Al_2O_3 is an excellent hydrogenation source for poly-Si passivating contacts [14], [18], [19]. It has been demonstrated that the chemical passivation from ALD Al_2O_3 on a poly-Si/SiO_2 stack roots from hydrogen diffusion (partially)

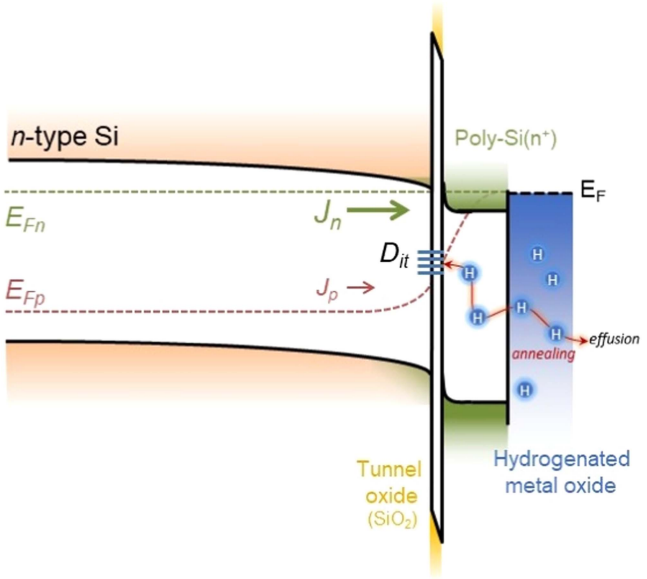

Fig. 1. Schematic of a poly-Si passivating contact consisting of n-type Si layer, ultrathin SiO_2 layer, and poly-Si (n^+) layer with a hydrogenated metal oxide overlayer. The surface passivation at SiO_2/c-Si(n) interface is achieved due to chemical passivation (hydrogenation) and field-effect passivation (carrier population control) thanks to band bending. The chemical passivation from metal oxides originates from hydrogen released from the metal oxide layer upon annealing, diffusing through the poly-Si to passivate the defects at SiO_2/c-Si(n) interface. The released hydrogen from the metal oxide layer can also diffuse to the surface of the metal oxide and effuse from the metal oxide (effusion). Note that for simplicity, the work functions of the poly-Si and the generic hydrogenated metal oxide were assumed to be equal in the schematic.

from the ALD layers hydrogenating the SiO_2/c-Si(n) interface to reduce the interfacial defects (see Fig. 1) [20]. Furthermore, it has been shown that ALD Al-doped ZnO on thin SiO_2 with Al_2O_3 capping is an excellent passivating contact for n^+ diffused doped Si surfaces [21], [22], [23]. In this case, hydrogenation of poly-Si enables an implied open-circuit voltage (iV_{OC}) of more than 735 mV [13]. In these studies, the Al_2O_3 capping layer was employed to prevent hydrogen effusion from the ZnO layer and enhance the optical and electrical quality of the ZnO [21], [22].

In this work, we explore the use of ALD nickel oxide (NiO) as a hydrogen source for poly-Si based contacts. While literature reports have so far focused on the hydrogenation via dielectrics or *n*-type metal oxides/transparent conductive oxides, NiO is a *p*-type metal oxide and as such widely used as a charge selective contact in solar cells. For example, NiO is already established as *p*-type contact layer in metal halide perovskite solar cells, by delivering conversion efficiency values as high as 21% [24]. By having a *p*-type contact layer, NiO can potentially be used in a tunnel recombination junction in tandem silicon/perovskite cells, which has recently been demonstrated in the literature [25]. Here, we demonstrate the hydrogenation of poly-Si(n)/SiO_2 contacts from ALD NiO and provide insights into this hydrogenation process. Furthermore, the passivation performance is tested on different poly-Si contact structures, where the doping level and thickness of the poly-Si layer are varied, as well as the surface finish (polished or textured). The reasons for these variations are as follows. First, hydrogenation is typically more critical for less doped poly-Si since the field effect is less pronounced. Second, passivation on textured surfaces is typically more challenging than polished surfaces, presumably due to the enhanced surface area and nanoscale roughness of the pyramids [26], [27]. Finally, thicker, highly doped poly-Si finds its industrial relevance in the i-TOPCon structure [28]. On the other hand, thin and less doped poly-Si is preferred on the front of the Si bottom cell in silicon-perovskite tandems, since this leads to less parasitic absorption of infrared light. Regarding the latter application, both planar and textured Si surfaces are currently pursued [29], [30], [31]. Furthermore, we include a comparison with the established ZnO/Al_2O_3 stack to aid the investigation of hydrogenation of the poly-Si stack by NiO.

Our results show that on planar wafers, hydrogenation from lowly doped poly-Si/ALD NiO stacks is highly effective and on par with ZnO/Al_2O_3, reaching iV_{OC} values of 730 mV. On textured wafers, hydrogenation is still effective (711 mV), yet lags behind the ZnO/Al_2O_3 stack (724 mV). By tracking the diffusion of hydrogen, it has been found that although NiO yields hydrogenation of the SiO_2 tunnel oxide, less hydrogen diffuses toward this interface during the annealing step, as compared to ZnO/Al_2O_3 capping layers. This is supported by effusion measurements, which show the onset of hydrogen effusion from NiO about 100 °C lower than for ZnO suggesting a higher loss of hydrogen before the optimal annealing temperature is reached. Building on this insight, it is shown that adding an Al_2O_3 capping layer to NiO significantly improves its hydrogenation performance on textured surfaces, resulting in an iV_{OC} of 728 mV.

II. Experiments

A. Sample Preparation

Poly-Si layers were deposited using low-pressure chemical vapor deposition (LPCVD). After standard RCA chemical surface cleaning of the wafer, a very thin thermal oxide layer was grown by in situ oxidation in the LPCVD process tube. Subsequently, an amorphous silicon layer was deposited by LPCVD from silane, in situ doped with phosphorus from PH_3. Note that the layer might be partially crystallized during the process at this step as reported from a previous study [32]. Finally, this layer was annealed in a tube furnace for crystallization into a polysilicon layer and to activate the dopants. Two types of poly-Si were used. One type was 140 nm thick with a doping level of 1.8×10^{20} cm^{-3} on a 4 Ω·cm Si(n) wafer, labeled as "thick, more doped poly-Si" onward. The other type was 65 nm with a doping level of 1×10^{20} cm^{-3} on a 2.5 Ω·cm Si(n) wafer, labeled as "thin, less doped poly-Si." Prior to the ALD metal oxide deposition, the poly-Si(n)/SiO_2/c-Si(n) wafers were treated in diluted hydrofluoric acid (1%) for 1 min to remove any surface oxide, then rinsed thoroughly with deionized water to remove any excess of hydrofluoric acid.

ALD of NiO was performed in a home-built ALD reactor with a base pressure of 5×10^{-6} mbar (the reactor is described in details elsewhere [33]). The process used nickel bis(N,N'-di-tert-butylacetamidinate) [Ni(^{t}Bu-MeAMD)$_2$] and water as coreactant. The precursor bubbler was kept at 90 °C and Ar

TABLE I
PROCESS DETAILS FOR ALD METAL OXIDES USED IN THIS WORK

Layer	Temper-ature (°C)	Reactor	Precursor (Dosing time/ Purging time)	Coreactant (Dosing time/ Purging time)	Growth per cycle (nm)
NiO	150	Home-built	Ni(^{t}Bu-MeAMD)$_2$ (8 s* / 20 s)	H_2O (0.1 s / 60 s)	0.045
ZnO	200	OpAL	DEZ (0.06 s / 5 s)	H_2O (0.06 s / 10 s)	0.16
Al_2O_3	200	OpAL	DMAI (0.2 s / 5 s)	H_2O (0.1 s / 10 s)	0.08

Note: *Two dosing steps in a closed chamber.

flow was used for bubbling. The precursor was first synthesized in a report by Li et al. [34] and subsequently used for ALD processes [35], [36], [37], however, no saturation curves were reported. Thus, a detailed study of the ALD NiO process will be presented in a separate publication. ALD of ZnO was performed in an Oxford Instruments OpAL ALD reactor using diethylzinc (DEZ) as precursor and water as coreactant. Details of the ALD ZnO process can be found in our previous publication [38]. ALD Al_2O_3 was prepared in the same reactor using dimethylaluminum isopropoxide (DMAI) and water as reported previously [39]. All the process parameters are summarized in Table I.

To study the hydrogenation, the c-Si(n)/SiO_2/poly-Si(n)/NiO and c-Si(n)/SiO_2/poly-Si(n)/ZnO/Al_2O_3 stacks were subjected to different annealing temperatures for 5 min in air on a hotplate up to 500 °C. For higher annealing temperatures, a rapid thermal annealing (RTA) setup was used where annealing was performed in N_2 (accumulated steps) at near-ambient pressure.

B. Characterization Methods

The lifetime measurements were performed with a Sinton Lifetime Tester WCT-120TS using transient/quasi-steady-state photoconductance decay measurements [40]. We extracted lifetime at an injection level of 10^{15} cm^{-3}, the implied open-circuit voltage at 1 sun illumination and the dark saturation current at an injection level of 5×10^{15} cm^{-3}. For these measurements, symmetrical lifetime samples were used.

Secondary ion mass spectrometry (SIMS) depth profiling was performed using an Ion-Tof TOF-SIMS IV instrument, operated in negative mode with 2-keV Cs^+ ions for sputtering. Depth scale calibration of the profiles was done on the basis of the total nominal thicknesses. A constant erosion rate in each sample and each layer was assumed, which introduces systematic errors up to a factor of 2 in the depth scale since different materials may have different erosion rates. Concentrations were calculated using literature values for the sensitivity factors in a Si matrix [41]. This implies that possible systematic errors are up to a factor of 3 for measurement on NiO, Al_2O_3, and ZnO layers. Nonetheless, within Si, the error of the concentrations is ±25%. Considering these estimated errors, it was not possible to quantify accurately the hydrogen concentration versus depth, however, qualitative changes in the hydrogen distribution profile can be discerned.

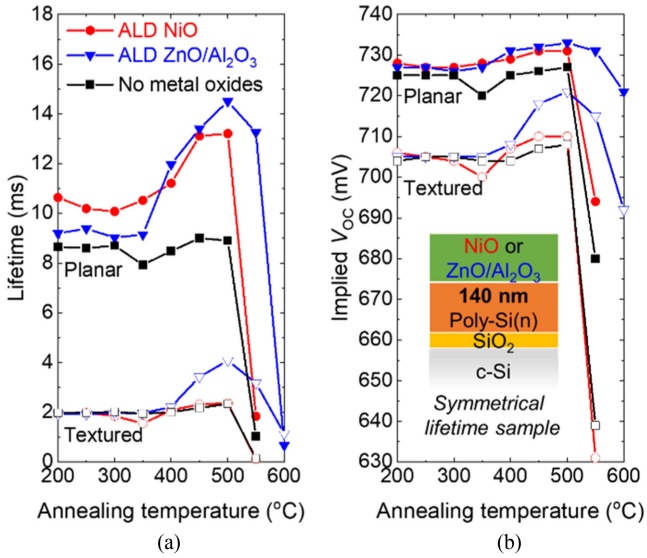

Fig. 2. (a) Minority charge carrier lifetime and (b) implied V_{OC} of poly-Si(n)/SiO_2/c-Si(n) (140 nm, doping concentration of 1.8×10^{20} cm^{-3}) stack with ALD metal oxide (7-nm NiO or 20-nm ZnO/20-nm Al_2O_3) and wafers without metal oxide layer. Filled symbols are polished wafers (planar) and open symbols are textured wafers. The wafers used were symmetrical samples of NiO/poly-Si(n)/SiO_2/c-Si(n) and Al_2O_3/ZnO/poly-Si(n)/SiO_2/c-Si(n) subjected to different annealing temperature for 5 min in ambient condition on a hotplate up to 500 °C (accumulated steps). Subsequent annealing steps (>500 °C) were done in a RTA system in N_2 atmosphere.

Hydrogen effusion measurements were performed by heating samples at a constant ramping rate of 20 °C/min in a quartz tube evacuated by a turbomolecular pump. The effused species were detected by a quadrupole-mass spectrometer. The setup was described in detail elsewhere [42]. For effusion measurements, symmetrical samples were prepared using polished FZ silicon wafers as substrates.

The optical properties of poly-Si layers were determined from spectroscopic ellipsometry (NIR (0.75–5 eV) Ellipsometer M2000, J.A. Woollam Company, Lincoln, NE, USA). Measurements were performed on Si wafers with a 100-nm-thick SiO_2 that serves to give an optical contrast between the Si wafer and poly-Si film. The poly-Si was modeled using two Tauc–Lorentz and one Drude oscillator to consider the contributions from bandgap and free carrier absorption, respectively.

Atomic force microscopy (AFM) imaging was carried out using a Veeco Dimension MultiMode microscope connected to a Nanoscope III controller in a tapping mode at the scan rate of 1 Hz using PPP-NCH probes (Nanosensors).

III. RESULTS AND DISCUSSION

A. Passivation Quality

Fig. 2 reports the minority charge carrier lifetime and iV_{OC} of the thick, more doped poly-Si stacks at different annealing temperatures. The c-Si(n)/SiO_2/poly-Si(n) stack without metal oxide overlayer (labeled as no metal oxides in the figure) exhibits an approximately constant lifetime of 9 ms during the annealing steps up to 500 °C. Although it has been reported that annealing

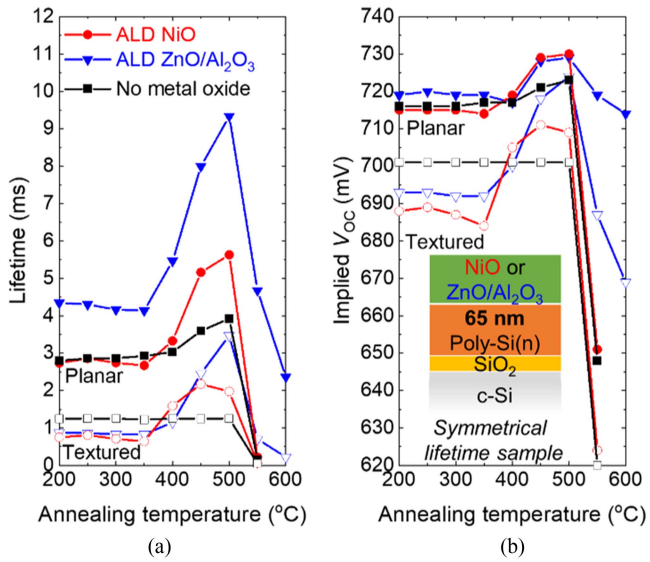

Fig. 3. (a) Minority charge carrier lifetime and (b) implied V_{OC} of poly-Si(n)/SiO_2/c-Si(n) (65 nm, doping concentration 1.0×10^{20} cm^{-3}) stack with ALD metal oxide (7-nm NiO or 20-nm ZnO/20-nm Al_2O_3) and wafers without metal oxides layer (black lines). Filled symbols are polished wafers (planar) and open symbols are textured wafers. The wafers used were symmetrical samples of NiO/poly-Si(n)/SiO_2/c-Si(n) and Al_2O_3/ZnO/poly-Si(n)/SiO_2/c-Si(n) subjected to different annealing temperature for 5 min in ambient condition on a hotplate up to 500 °C (accumulated steps). Subsequent annealing steps (>500 °C) were done in a RTA system in N_2 atmosphere.

in air can improve the iV_{OC} of poly-Si stack due to positive effect of water vapor in annealing environment [43], [44], in our case, the iV_{OC} stays constant without metal oxide layers. In contrast, as can been seen in Fig. 2(a), the minority charge lifetime increases from 350 °C for the stack with a 7-nm NiO layer. For polished wafers, the lifetime reaches 13.2 ms for NiO at an optimal annealing temperature of 500 °C, corresponding to an excellent iV_{OC} value of 731 mV [see Fig. 2(b)]. On the other hand, the lifetimes obtained on textured wafers are generally lower and only a modest improvement in lifetime is obtained for the sample with a NiO layer. After annealing at 500 °C, lifetime and iV_{OC} values of 2.4 ms and 710 mV have been achieved, respectively. These values are very similar to the reference wafer without a metal oxide capping layer, suggesting that the hydrogenation by NiO on these textured wafers is ineffective.

Fig. 3 displays the passivation results for a very similar experiment, in which thinner and less doped poly-Si was used. The thinner and lower doping level allow for better transparency in the IR region due to lower free charge carrier absorption in agreement to a previous report [45]. As can be seen in Fig. 3(a), the initial lifetime of the bare planar thin, less doped poly-Si stack is lower compared to thick, more doped poly-Si stack (3 ms *versus* 9 ms for planar wafers). This is most likely related to a lower field-effect passivation of thinner less doped poly-Si layer compared to the thicker more doped counterpart. Hence, it is expected that hydrogenation plays a more crucial role in thin poly-Si stacks to achieve a high minority charge carrier lifetime and high iV_{OC}. Indeed, as can be seen from Fig. 3(b) for thin, less doped poly-Si/NiO samples, a stronger increment in iV_{OC} can be seen compared to the thick, more doped poly-Si/NiO stacks [see Fig. 2(b)]. For polished wafers, the improvement is roughly 15 mV, whereas for textured wafers, the improvement in iV_{OC} is significant, increasing by 23 mV for the poly-Si/NiO-based stack. This highlights the vital role of hydrogenation in a thin, less doped poly-Si stack to achieve high iV_{OC} compared to the thick, more doped poly-Si. Also note that although dopant deactivation by hydrogen has been reported in [46], [47], and [48], annealing induces a reduction in sheet resistance of the stack from 71.1 to 61.5 Ω/□. This is likely due to an increase in conductivity of the poly-Si upon annealing. Hence, we do not expect dopant deactivation by hydrogen and accompanying decrease in field-effect passivation in this case.

In Figs. 2(a) and 3(a), beyond the annealing temperature at 450–500 °C, the passivation quality decreases with further annealing. This trend is most likely related to the loss of hydrogen from the SiO_2/c-Si(n) interface. It has been reported that Si–H bonds are broken upon annealing at 550 °C, thereby increasing the surface trap state density [49]. Moreover, annealing steps up to 500 °C were carried out in ambient atmosphere whereas subsequent annealing steps were done in N_2 atmosphere. To examine the effect of annealing atmosphere, we compare the lifetime values of wafers annealing in ambient condition and annealing in N_2. We observe that annealing in N_2 degrades the bare wafer faster than annealing in air as the lifetime of the minority charge carrier rapidly decreases already from 400 °C annealing temperature onward in N_2 atmosphere. Therefore, both effects of high temperature and annealing atmosphere are likely to explain the passivation quality loss shown in the lifetime test. We acknowledge that the initial lifetime values are different from different investigated wafers, which can be likely attributed to the variation in processing and handling, however, considering that the achieved value after annealing is higher than initial value as well as values obtained in bare wafers (without ALD metal oxide), we trust that ALD metal oxides effectively hydrogenate the poly-Si stacks on polished wafers.

Figs. 2 and 3 additionally show passivation results for samples capped with an ALD ZnO/Al_2O_3 stack. Similar to NiO stacks, the lifetime of the sample with a ZnO/Al_2O_3 stack exhibits a constant lifetime up to 350 °C, then the lifetime values increase rapidly. Interestingly, better passivation results are obtained for this stack, suggesting a better degree of hydrogenation. Especially on textured surfaces, the difference is pronounced, where the ZnO/Al_2O_3 stack achieves on the order of 10-mV higher iV_{oc} values. To elucidate the hydrogenation mechanism from ALD NiO layers and to gain insights into the observed passivation differences between NiO and ZnO/Al_2O_3 stacks, the remainder of this work focuses on dedicated studies of hydrogen within these stacks and how this evolves upon thermal annealing.

B. Role of Hydrogen Content

The first consideration for an effective hydrogenation from a metal oxide is its hydrogen content. In other words, it can be expected that higher lifetimes can be achieved with thicker layers, which is evidenced in the comparison of different thicknesses of the metal oxide, i.e., capping with 20-nm ZnO performs better than 7-nm ZnO.

TABLE II
ERD RESULT OF DIFFERENT ALD LAYERS MEASURED ON 20-NM LAYERS DEPOSITED ON CZ WAFERS

	20-nm NiO	20-nm ZnO/ 20-nm Al_2O_3
Total areal H content (10^{15} atoms per cm^2)	31±2	13±0.9
Average hydrogen concentration (10^{22} atoms per cm^3)	1.6±0.1	0.3±0.02

Elastic recoil detection (ERD) was used to quantify the amount of hydrogen in as-deposited (pristine) metal oxide layers. The hydrogen atomic areal densities of the ALD metal oxides are presented in Table II. In this case, the thickness of NiO is 20 nm so that the signal of NiO can be distinguished clearly from the layers' underneath. ERD shows that 20-nm NiO has 31×10^{15} hydrogen atoms/cm^2 corresponding to a hydrogen concentration of 1.6×10^{22} cm^{-3}, which is higher than the hydrogen concentration in ZnO/Al_2O_3 at a value of 0.3×10^{22} cm^{-3}. Although the spatial sensitivity of ERD is limited to about 20 nm, the peak position can indicate whether the hydrogen is concentrated mainly on the surface of NiO or distributed homogeneously. The simulated ERD spectra of the hydrogen profile in NiO show that hydrogen is distributed homogeneously throughout the layer. Thus, it is valid to assume a linear dependence between the amount of hydrogen and the film thickness. Therefore, a 7 nm (similar to the thickness value used in lifetime test) thick NiO film would likely have 11×10^{15} hydrogen atoms/cm^2, which is slightly less than 13×10^{15} hydrogen atoms/cm^2 present in the ZnO/Al_2O_3 layer. However, this difference is only marginally higher than the error presented in Table II, hence, the total hydrogen content in the pristine metal oxides seems not to play a decisive role in the differences in observed lifetime. Furthermore, note that this high hydrogen content in ALD metal oxides is a few orders of magnitude higher than the interfacial defect density on the surface of Si—of the order of 10^{12} cm^{-2} [15]. Therefore, we hypothesize that the total hydrogen concentration in the ALD metal oxides is not the sole reason behind the difference seen in passivation tests.

C. Role of Hydrogen Retainment in the Layers

Previous reports have demonstrated a clear link between hydrogen concentration at the SiO_2/c-Si interface and the achieved surface passivation, where higher hydrogen concentration seen in SIMS has been coupled with better lifetime of the investigated stacks [21], [50]. Hence, SIMS was employed to detect the hydrogen redistribution due to annealing. SIMS analysis of the NiO/poly-Si(n)/SiO_2/c-Si(n) stack is shown in Fig. 4, both in the pristine state and after annealing. We further use a similar thickness of 20-nm NiO in subsequent characterizations to ensure a high hydrogen content in NiO, on par with ZnO/Al_2O_3 to examine other underlining factors affecting hydrogenation besides total hydrogen content.

Fig. 4(a) shows the pristine layer (prior to annealing), whereas Fig. 4(b) presents the elemental traces after annealing at 500 °C in air, which gives the optimal passivation. Comparing the hydrogen profiles before and after annealing can provide

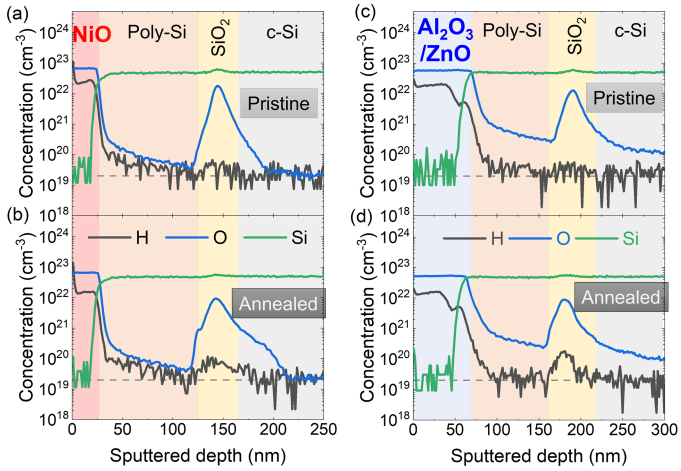

Fig. 4. SIMS of (a) pristine and (b) after annealing at 500 °C for 5 min in air of NiO/poly-Si(n)/SiO_2/c-Si(n) stack; (c) pristine and (d) after annealing at 500 °C for 5 min in air of Al_2O_3/ZnO/poly-Si(n)/SiO_2/c-Si(n) stack. The blue trace is O, black trace is H, and green trace is Si signal. The color scheme is to guide the eyes toward different layers as inferred from the Si and O signals. The dashed line is to indicate the background H level. Note that the NiO layer thickness is 20 nm in this measurement to ensure no limitation from hydrogen content as explained earlier.

evidence for chemical passivation. The oxygen and silicon signals are plotted alongside the hydrogen signal, which helps to identify the layers, as shown in different color schemes in Fig. 4. The yellow layer can be assigned to SiO_2 due to a strong signal of oxygen, which is significantly higher than the values in adjacent layers namely poly-Si and c-Si layers. Even though SiO_2 is ultrathin (on the order of 1–2 nm), the oxygen signal is broadened significantly, most likely due to nonuniformity of the etch front. Moreover, since the used planar wafers are not mirror polished (the rms roughness value of around 264 nm obtained from AFM scan), additional broadening of the signal might be expected. However, we believe that the qualitative change of the trend is valid when comparing wafers before and after annealing.

As can be seen in Fig. 4, the hydrogen concentration is low throughout the stacks except for the ALD metal oxides. The background hydrogen level (indicated by the dashed line) is around 2×10^{19} cm^{-3}, as can be seen in the poly-Si and c-Si regions. A slightly higher hydrogen concentration in the SiO_2 region compared to the Si regions can be seen in the pristine NiO stack, however, the signal is relatively noisy. When the NiO stack is annealed at 500 °C in ambient condition, it can be seen that the hydrogen content in the annealed NiO layer [depicted as red area in Fig. 4(b)] is slightly lower compared to the pristine stack [see Fig. 4(a)]. Notably, after annealing at 500 °C, a slight increase of H concentration at SiO_2/c-Si(n) interface can be seen in Fig. 4(b). We note that SIMS measurement is inadequate to clearly distinguish whether hydrogen content increases within the SiO_2 layer or at the SiO_2 interface with the c-Si layer. Nonetheless, the improvement in minority charge carrier lifetime and iV_{OC} after annealing indicates that chemical passivation occurs at SiO_2/c-Si(n) interface, as also reported in the literature [51]. Even though the increment of hydrogen content at the SiO_2/c-Si(n) interface of the NiO stack is modest reaching 1×10^{20} cm^{-3}, the peak is visible compared

to the background level and the signal is less noisy compared to pristine case [see Fig. 4(a)]. Thus, it is strongly evident that NiO can provide hydrogen for chemical passivation of poly-Si(*n*)/SiO_2/c-Si(*n*)stack.

Fig. 4(c) shows the pristine wafer with the ZnO/Al_2O_3 stack. We observe a similar hydrogen background level in this stack. Upon annealing, comparing to the NiO case, the decrease in H content is less in ZnO/Al_2O_3 layers [see Fig. 4(d)]. This is likely due to the effective Al_2O_3 capping layer to prevent H effusion from ZnO. This result is in agreement with a previous report, where Al_2O_3 capping reduces significant H effusion signal from ZnO [21]. Comparing the black trace between Fig. 4(c) and (d), the hydrogen content increases clearly at the SiO_2/c-Si(*n*) interface after annealing. Here, the annealed ZnO/Al_2O_3 sample shows a clear peak of hydrogen at the region identified as SiO_2 layer similar to previous observations [21], [52]. This increase in hydrogen content is more pronounced in ZnO/Al_2O_3 compared to the NiO case [see Fig. 4(b) and (d)] and can explain the higher obtained lifetime for ZnO/Al_2O_3 stacks. For both poly-Si stacks, the hydrogen content stays low in the poly-Si layer before or after 500 °C annealing near the SIMS detection limit of about 10^{19} cm^{-3}. We note, however, that this lack of high hydrogen trapping levels does not contradict hydrogen diffusion through the poly-Si. Reported hydrogen concentration levels in poly-Si arising from solid diffusion source layers are also in the range of 1–3 × 10^{19} cm^{-3} [53].

As the SIMS results show a loss in hydrogen content of NiO after high temperature annealing, we used effusion measurements to detect the effused gases from the layers upon high temperature annealing. Effusion measurements have proven useful to understand the hydrogenation of various systems reported in the literature, where the hydrogen effusion signal can indicate the temperature at which hydrogen atoms become mobile and also provide an insight into the hydrogen content of different layers [14], [21], [42], [54]. Similar to SIMS, effusion measurements were done with 20-nm NiO for a direct comparison. Note, however, that the investigated stacks did not involve the poly-Si layer. Fig. 5 presents the effusion results from NiO deposited symmetrically on a float zone Si wafer. Fig. 5(a) shows the hydrogen (mass 2) and water (mass 18) effusion rates as a function of temperature. Fig. 5(b) presents the quantification of effusion rate of hydrogen (dN_H/dt). A pronounced effusion spike for both species is observed at a temperature near 300 °C. Since for detection of molecules by the quadrupole mass analyzer, a heated filament and a voltage of about 80 V were used for ionization by electron impact, the hydrogen signal could, in principle, arise from the fractionation of water in the ionization process. However, fractionation of water in the same effusion system gives ratios of mass 18 to mass 2 signals exceeding two orders of magnitude, whereas in the present case shown in Fig. 5(a), this ratio is about 2. Thus, the effusion spikes of hydrogen and water must have a different nature. It appears likely that hydrogen is incorporated in NiO predominantly in various hydroxyl groups. For instance, Koushik et al. [55] reported for ALD NiO surfaces the presence of NiOOH and $Ni(OH)_2$ species and a decrease of their signal upon annealing at 300 °C based on X-ray photonelectron spectroscopy

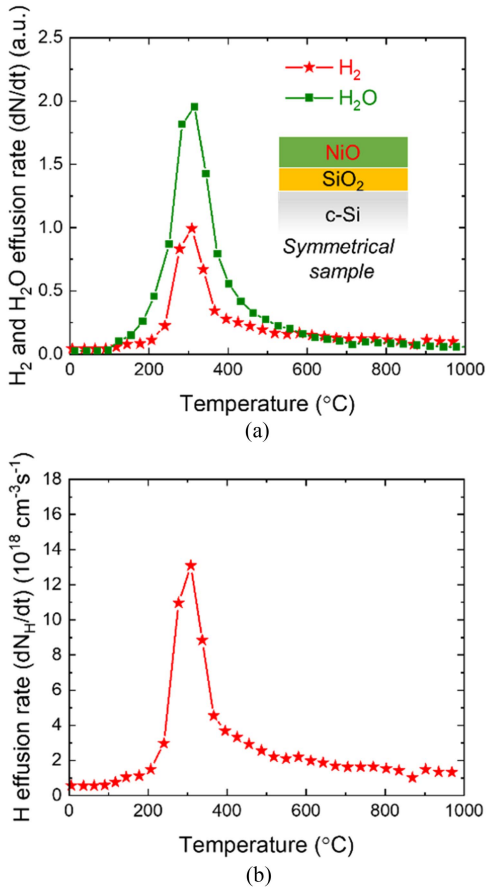

Fig. 5. Effusion results of 20-nm ALD NiO on an FZ Si wafer (symmetrical samples—double sided deposition) using a 20 °C/min temperature ramp. (a) Red trace is hydrogen and green trace is H_2O effusion rate. (b) Quantified hydrogen effusion rate, i.e., hydrogen atoms per volume per time.

measurements. Elbaz et al. [56] reported for various nickel oxy/hydroxyl materials the diffusion of atomic hydrogen. The release of water upon annealing was reported for various Ni hydroxyl materials [57], [58], [59], [60]. In three of these studies, a H_2O desorption temperature near 300 °C was also found [58], [59], [60].

However, such a dehydroxylation process cannot explain why the hydrogen and water effusion spikes occur at the same temperature. As H_2O molecules are too large to effuse from a compact material [42], we expect that the water desorption comes either from the film surface or from internal voids where water is trapped. One possibility is that part of the (interstitial) hydrogen, which diffuses toward the surface, reduces the NiO there, and forms H_2O, resulting in the H_2O effusion spike. Evidence for the reduction of NiO by hydrogen has been reported in the literature at similar temperature ranges [59]. However, our SIMS data (within accuracy) show no evidence for NiO reduction. Yet, as the SIMS data was obtained from samples annealed in ambient (as opposed to vacuum annealing for effusion), it is well possible that any reduction of NiO by hydrogen is counteracted by oxidation from the ambient.

Another possibility is that the diffusing hydrogen (and desorbing H_2O) gets trapped in voids, which may open up at high

pressure releasing both H_2O and H_2. Both models thus can explain the simultaneous H_2 and H_2O effusion peaks. Support for the presence of water molecules within the NiO comes also from a comparison of the hydrogen content measured by hydrogen effusion and ERD. Integration over the hydrogen effusion curve in Fig. 5(b) gives about 0.5×10^{22} cm^{-3} hydrogen atoms in the layer. Note that this number is lower than the ERD result (1.6×10^{22} cm^{-3}), which indicates that there might be some water trapped in the grain boundaries of the layer. Since the ERD result can be influenced by hydrogen in water molecules, whereas water molecules cannot contribute to the hydrogen effusion results (in the effusion spike), trapped water molecules might be present in the layer. Furthermore, some fraction of hydrogen in the layer is also expected to contribute to the H_2O effusion spike, which can further explain the difference between effusion and ERD measurements. The pronounced effusion of hydrogen (and water) starting around 200 °C shows that hydrogen in the NiO becomes mobile at rather low temperatures. In combination with the SIMS data interpretation earlier, we postulate that hydrogen from the NiO upon annealing can partially effuse to the ambient and partially diffuse inside the stack resulting in chemical passivation.

This study shows that the main hydrogen effusion from NiO starts near 200 °C, whereas previous work showed that hydrogen effusion from ZnO starts at about 100 °C higher temperatures, despite that similar process temperatures (150 °C/200 °C) had been applied [21], [38]. This indicates that the energy barriers for the mobilization and surface desorption of hydrogen for these two metal oxides are not the same. Using the relation between H effusion temperature and Arrhenius dependence ($D = D_0 \exp(-E_D/kT)$, with D the diffusion coefficient, D_0 the diffusion prefactor, E_D the activation energy for diffusion, and k Boltzmann's constant) of hydrogen diffusion [61], one can estimate the involved hydrogen diffusion energies by assuming a hydrogen diffusion prefactor. Using the theoretical diffusion prefactor $D_0 = 10^{-3}$ cm^2/s as often assumed [42], [53] activation energies of 1.36 eV for the ZnO and 1.27 eV for the NiO are obtained. Nonetheless, we observe a similar trend and a similar optimal temperature of passivation in Figs. 2 and 3 for the NiO and ZnO/Al_2O_3 stacks. Moreover, even though both the thicknesses and the doping levels are different in the data of the mentioned figures, the lifetime and iV_{OC} increase with similar trends as a function of annealing temperatures. There are two likely mechanisms that can contribute to this similarity.

First, such similar behavior is to be expected if the diffusion of hydrogen through the poly Si layers plays an important role. Using the poly-Si layer thicknesses of the stacks and H diffusion data for poly-Si with randomly distributed grain boundaries by Nickel et al. [53] ($D_0 = 10^{-3}$ and 4×10^{-3} cm^2/s, $E_D = 1.50$ and 1.69 eV), respectively, one can estimate the temperature of maximum H effusion, i.e., the temperature of maximum flow of hydrogen toward the c-Si interface [61]. For the stack of Fig. 2, 485–505 °C is obtained, for the stack of Fig. 3, 450–460 °C. Thus, the differences in the lifetime maxima in Figs. 2 and 3 agree quite well with this result and suggest that passivation depends on the temperature (and time) required for hydrogen diffusion inside poly-Si to reach SiO_2/c-Si(n) interface for chemical passivation [53], [62].

A second likely mechanism is the presence of a separate energy barrier for hydrogenation of the SiO_2/c-Si(n) interface aside from the temperature required for hydrogen to diffuse through the poly-Si. In related work from our group, the passivation by c-Si/SiO_2/ZnO:Al/Al_2O_3 stacks has been studied, which closely resemble the c-Si/SiO_2/poly-Si(n)/ZnO:Al/Al_2O_3 stacks of [21], [22], and [23]. While in that case, the hydrogen present in the ZnO:Al does not have to diffuse through the poly-Si, very similar optimal annealing temperatures for passivation were found in the range of 450–500 °C. Importantly, it has been observed that the annealing temperature at which the passivation is activated does depend on the preparation method of the ultrathin SiO_2. This implies that also the SiO_2 layer plays a role in the activation temperature, although the exact nature of the associated energy barrier is difficult to pinpoint.

Looking at the decay of passivation quality at temperatures exceeding the optimal annealing temperatures, it can readily be seen that the ZnO/Al_2O_3 stacks yield better thermal stability as compared to the NiO layer. This is attributed to the much greater loss of hydrogen from the NiO layer as compared to the ZnO/Al_2O_3 layer during annealing.

The discussion on the effusion measurements and SIMS data both show that a substantial amount of hydrogen is lost prior to the optimal passivation temperature. It is worth noting that the hydrogen reduction seen in SIMS data before and after annealing is only about half, whereas about 80% of the amount of hydrogen of the total quantified amount of hydrogen in the effusion measurement (going up to 1000 °C) is already lost prior to 500 °C. This difference suggests that even as 1000 °C, the NiO films still contain hydrogen, most likely trapped as H_2O or H_2 in voids. A high stability of trapped molecules in voids is well known from a-Si:H at 1000 °C [42] and more is needed for effusion of argon, which is of smaller size than H_2O, from a-SiO_x [42]. However, these H_2O and H_2 molecules trapped in voids in NiO at temperatures near 500 °C and above are not considered to contribute to the surface passivation.

D. *Effective Capping by Al_2O_3*

Aiming to retain the hydrogen in the NiO layer and prevent hydrogen loss before the optimal annealing temperature, a 20-nm Al_2O_3 capping layer on NiO was employed to prevent hydrogen effusion from this layer, as Al_2O_3 has been demonstrated to be an effective capping layer for ZnO [21]. Furthermore, it has been shown in the literature that Al_2O_3 can supply additional hydrogen for chemical passivation [50]. Here, we focus on the textured wafers as it is more challenging to achieve good passivation of textured wafers compared to the planar counterpart. The Al_2O_3 capping on NiO increases the iV_{OC} compared to NiO alone for both poly-Si stacks, reaching more than 717 mV for thick poly-Si and excellent value of 728 mV for thin poly-Si. This confirms that an additional Al_2O_3 layer can (either) prevent hydrogen effusion from NiO, and/or supply additional hydrogen to achieve better surface passivation. Therefore, although a large amount of hydrogen is present in NiO, it is crucial to keep the hydrogen

within the stack until the temperature needed for activation of the surface passivation is reached.

IV. Conclusion

It has been demonstrated in this study that ALD NiO can be a good hydrogen source for chemical passivation of poly-Si(n)/SiO_2/c-Si(n) stacks. Evidenced from lifetime measurements, we found that ALD NiO can improve the minority charge carrier lifetime and implied open-circuit voltage upon annealing. SIMS measurements demonstrate that the chemical passivation from NiO originates from the increment of hydrogen at SiO_2/c-Si(n) surface. However, despite being richer in hydrogen, we found that for NiO, this increment in hydrogen at the interface was less than for the ZnO/Al_2O_3 stack, explaining the higher iV_{OC} values achieved for the latter. The relatively lower hydrogenation performance of NiO was linked to substantial hydrogen effusion from the layer at temperatures below the optimal temperature for activation of the surface passivation. Hence, to prevent hydrogen effusion, Al_2O_3 capping on NiO was used, which resulted in excellent value of 728-mV iV_{OC} for the thin, less-doped poly-Si stack. These results underline the potential to use ALD metal oxides, including p-type metal oxide, for hydrogenation of poly-Si stacks.

Acknowledgment

The authors would like to thank Barathi Krishnamoorthy, Caspar van Bommel, Joris Meulendijks, and Janneke Zeebregts at TU/e for the technical support. The authors would also like to thank Dr. Wim Arnold-Bik at Detect99 for performing ERD measurement, Hans Snijders and Dr. Jurgen van Berkum (Eurofins Materials Science Netherlands B.V.) for acquiring SIMS data, and Dr. Dibyashree Koushik and Dr. Michael McMaster (TU/e) for assisting the deposition of ALD NiO. Mariadriana Creatore acknowledges the NWO Aspasia Program.

References

[1] T. G. Allen, J. Bullock, X. Yang, A. Javey, and S. De Wolf, "Passivating contacts for crystalline silicon solar cells," *Nature Energy*, vol. 4, no. 11, pp. 914–928, Nov. 2019, doi: 10.1038/s41560-019-0463-6.

[2] J. Melskens et al., "Passivating contacts for crystalline silicon solar cells: From concepts and materials to prospects," *IEEE J. Photovolt.*, vol. 8, no. 2, pp. 373–388, Mar. 2018, doi: 10.1109/JPHOTOV.2018.2797106.

[3] A. Cuevas et al., "Carrier population control and surface passivation in solar cells," *Sol. Energy Mater. Sol. Cells*, vol. 184, pp. 38–47, 2018, doi: 10.1016/j.solmat.2018.04.026.

[4] R. Brendel and R. Peibst, "Contact selectivity and efficiency in crystalline silicon photovoltaics," *IEEE J. Photovolt.*, vol. 6, no. 6, pp. 1413–1420, Nov. 2016, doi: 10.1109/JPHOTOV.2016.2598267.

[5] J. I. Michel, J. Dréon, M. Boccard, J. Bullock, and B. Macco, "Carrier-selective contacts using metal compounds for crystalline silicon solar cells," *Prog. Photovolt.: Res. Appl.*, pp. 1–34, Mar. 2022, doi: 10.1002/pip.3552.

[6] A. Richter et al., "n-type Si solar cells with passivating electron contact: Identifying sources for efficiency limitations by wafer thickness and resistivity variation," *Sol. Energy Mater. Sol. Cells*, vol. 173, pp. 96–105, Dec. 2017, doi: 10.1016/j.solmat.2017.05.042.

[7] F. Haase et al., "Laser contact openings for local poly-Si-metal contacts enabling 26.1%-efficient POLO-IBC solar cells," *Sol. Energy Mater. Sol. Cells*, vol. 186, pp. 184–193, Nov. 2018, doi: 10.1016/j.solmat.2018.06.020.

[8] A. Richter et al., "Design rules for high-efficiency both-sides-contacted silicon solar cells with balanced charge carrier transport and recombination losses," *Nature Energy*, vol. 6, no. 4, pp. 429–438, Apr. 2021, doi: 10.1038/s41560-021-00805-w.

[9] Trina Solar, "Trina solar announces new efficiency record of 23.22% with n-type i-TOPCon solar cell on Cast-mono substrate," 2019. Accessed: Oct. 15, 2021. [Online]. Available: https://www.trinasolar.com/en-glb/resources/newsroom/matrina-solar-announces-new-efficiency-record-2322-n-type-i-topcon-solar-cell

[10] T. N. Truong et al., "Hydrogenation of phosphorus-doped polycrystalline silicon films for passivating contact solar cells," *ACS Appl. Mater. Interfaces*, vol. 11, no. 5, pp. 5554–5560, Feb. 2019, doi: 10.1021/acsami.8b19989.

[11] M. Hermle, F. Feldmann, M. Bivour, J. C. Goldschmidt, and S. W. Glunz, "Passivating contacts and tandem concepts: Approaches for the highest silicon-based solar cell efficiencies," *Appl. Phys. Rev.*, vol. 7, no. 2, Jun. 2020, Art. no. 021305, doi: 10.1063/1.5139202.

[12] D. Yan et al., "Polysilicon passivated junctions: The next technology for silicon solar cells?," *Joule*, vol. 5, no. 4, pp. 811–828, Apr. 2021, doi: 10.1016/j.joule.2021.02.013.

[13] L. Tutsch et al., "Improved passivation of n-type poly-Si based passivating contacts by the application of hydrogen-rich transparent conductive oxides," *IEEE J. Photovolt.*, vol. 10, no. 4, pp. 986–991, Jul. 2020, doi: 10.1109/JPHOTOV.2020.2992348.

[14] G. Dingemans, W. Beyer, M. C. M. Van De Sanden, and W. M. M. Kessels, "Hydrogen induced passivation of Si interfaces by Al_2O_3 films and SiO_2/Al_2O_3 stacks," *Appl. Phys. Lett.*, vol. 97, no. 15, 2010, Art. no. 152106, doi: 10.1063/1.3497014.

[15] J. Melskens et al., "Excellent passivation of n-Type silicon surfaces enabled by pulsed-flow plasma-enhanced chemical vapor deposition of phosphorus oxide capped by aluminum oxide," *Phys. Status Solidi–Rapid Res. Lett.*, vol. 15, no. 1, Jan. 2021, Art. no. 2000399, doi: 10.1002/pssr.202000399.

[16] J. Cui et al., "Highly effective electronic passivation of silicon surfaces by atomic layer deposited hafnium oxide," *Appl. Phys. Lett.*, vol. 110, no. 2, Jan. 2017, Art. no. 021602, doi: 10.1063/1.4973988.

[17] B. Liao, B. Hoex, A. G. Aberle, D. Chi, and C. S. Bhatia, "Excellent c-Si surface passivation by low-temperature atomic layer deposited titanium oxide," *Appl. Phys. Lett.*, vol. 104, no. 25, Jun. 2014, Art. no. 253903, doi: 10.1063/1.4885096.

[18] B. W. H. van de Loo et al., "On the hydrogenation of Poly-Si passivating contacts by Al_2O_3 and SiN_x thin films," *Sol. Energy Mater. Sol. Cells*, vol. 215, 2020, Art. no. 110592, doi: 10.1016/j.solmat.2020.110592.

[19] G. Yang et al., "Passivation enhancement of poly-Si carrier-selective contacts by applying ALD Al_2O_3 capping layers," *IEEE J. Photovolt.*, vol. 12, no. 1, pp. 259–266, Jan. 2022, doi: 10.1109/JPHOTOV.2021.3119595.

[20] M. Schnabel et al., "Hydrogen passivation of poly-Si/SiO_x contacts for Si solar cells using Al_2O_3 studied with deuterium," *Appl. Phys. Lett.*, vol. 112, no. 20, 2018, Art. no. 203901, doi: 10.1063/1.5031118.

[21] B. W. H. van de Loo, B. Macco, J. Melskens, W. Beyer, and W. M. M. Kessels, "Silicon surface passivation by transparent conductive zinc oxide," *J. Appl. Phys.*, vol. 125, no. 10, 2019, Art. no. 105305, doi: 10.1063/1.5054166.

[22] B. Macco et al., "Atomic-layer-deposited Al-doped zinc oxide as a passivating conductive contacting layer for n+-doped surfaces in silicon solar cells," *Sol. Energy Mater. Sol. Cells*, vol. 233, Dec. 2021, Art. no. 111386, doi: 10.1016/j.solmat.2021.111386.

[23] B. Macco et al., "Temporal and spatial atomic layer deposition of Al-doped zinc oxide as a passivating conductive contact for silicon solar cells," *Sol. Energy Mater. Sol. Cells*, vol. 245, Sep. 2022, Art. no. 111869, doi: 10.1016/j.solmat.2022.111869.

[24] W. Chen et al., "Alkali chlorides for the suppression of the interfacial recombination in inverted planar perovskite solar cells," *Adv. Energy Mater.*, vol. 9, no. 19, May 2019, Art. no. 1803872, doi: 10.1002/aenm.201803872.

[25] J. Kim et al., "Potential of NiO_x/Nickel Silicide/n^+ poly-Si contact for Perovskite/TOPCon tandem solar cells," *Energies*, vol. 15, no. 3, Jan. 2022, Art. no. 870, doi: 10.3390/en15030870.

[26] K. R. McIntosh and L. P. Johnson, "Recombination at textured silicon surfaces passivated with silicon dioxide," *J. Appl. Phys.*, vol. 105, no. 12, Jun. 2009, Art. no. 124520, doi: 10.1063/1.3153979.

[27] H. Angermann et al., "Optimisation of electronic interface properties of a-Si:H/c-Si hetero-junction solar cells by wet-chemical surface pretreatment," *Thin Solid Films*, vol. 516, no. 20, pp. 6775–6781, Aug. 2008, doi: 10.1016/j.tsf.2007.12.033.

[28] Y. Chen et al., "Mass production of industrial tunnel oxide passivated contacts (i-TOPCon) silicon solar cells with average efficiency over 23% and modules over 345 W," *Prog. Photovolt.: Res. Appl.*, vol. 27, no. 10, pp. 827–834, Oct. 2019, doi: 10.1002/pip.3180.

[29] M. Jošt et al., "Textured interfaces in monolithic perovskite/silicon tandem solar cells: Advanced light management for improved efficiency and energy yield," *Energy Environ. Sci.*, vol. 11, no. 12, pp. 3511–3523, 2018, doi: 10.1039/C8EE02469C.

[30] A. Al-Ashouri et al., "Monolithic perovskite/silicon tandem solar cell with >29% efficiency by enhanced hole extraction," *Science*, vol. 370, no. 6522, pp. 1300–1309, Dec. 2020, doi: 10.1126/science.abd4016.

[31] F. H. Isikgor et al., "Concurrent cationic and anionic perovskite defect passivation enables 27.4% perovskite/silicon tandems with suppression of halide segregation," *Joule*, vol. 5, no. 6, pp. 1566–1586, Jun. 2021, doi: 10.1016/j.joule.2021.05.013.

[32] M. K. Stodolny et al., "Material properties of LPCVD processed n-type polysilicon passivating contacts and its application in PERPoly industrial bifacial solar cells," *Energy Procedia*, vol. 124, pp. 635–642, Sep. 2017, doi: 10.1016/j.egypro.2017.09.250.

[33] S. B. S. Heil, E. Langereis, F. Roozeboom, M. C. M. van de Sanden, and W. M. M. Kessels, "Low-temperature deposition of TiN by plasma-assisted atomic layer deposition," *J. Electrochem. Soc.*, vol. 153, no. 11, 2006, Art. no. G956, doi: 10.1149/1.2344843.

[34] Z. Li, R. G. Gordon, V. Pallem, H. Li, and D. V. Shenai, "Direct-liquid-injection chemical vapor deposition of nickel nitride films and their reduction to nickel films," *Chem. Mater.*, vol. 22, no. 10, pp. 3060–3066, May 2010, doi: 10.1021/cm903636j.

[35] E. Thimsen, A. B. F. Martinson, J. W. Elam, and M. J. Pellin, "Energy levels, electronic properties, and rectification in ultrathin p-NiO films synthesized by atomic layer deposition," *J. Phys. Chem. C*, vol. 116, no. 32, pp. 16830–16840, Aug. 2012, doi: 10.1021/jp302008k.

[36] C.-C. Hsu, H.-W. Su, C.-H. Hou, J.-J. Shyue, and F.-Y. Tsai, "Atomic layer deposition of NiO hole-transporting layers for polymer solar cells," *Nanotechnology*, vol. 26, no. 38, Sep. 2015, Art. no. 385201, doi: 10.1088/0957-4484/26/38/385201.

[37] R. Zhao, S. Xiao, S. Yang, and X. Wang, "Surface thermolytic behavior of nickel amidinate and its implication on the atomic layer deposition of nickel compounds," *Chem. Mater.*, vol. 31, no. 14, pp. 5172–5180, 2019, doi: 10.1021/acs.chemmater.9b01267.

[38] B. Macco et al., "Atomic layer deposition of high-mobility hydrogen-doped zinc oxide," *Sol. Energy Mater. Sol. Cells*, vol. 173, pp. 111–119, Dec. 2017, doi: 10.1016/j.solmat.2017.05.040.

[39] S. E. Potts, G. Dingemans, C. Lachaud, and W. M. M. Kessels, "Plasma-enhanced and thermal atomic layer deposition of Al_2O_3 using dimethylaluminum isopropoxide, $[Al(CH_3)_2\ (\mu\text{-}O^iPr)]_2$, as an alternative aluminum precursor," *J. Vac. Sci. Technol. A*, vol. 30, no. 2, Mar. 2012, Art. no. 021505, doi: 10.1116/1.3683057.

[40] R. A. Sinton and A. Cuevas, "Contactless determination of current–voltage characteristics and minority-carrier lifetimes in semiconductors from quasi-steady-state photoconductance data," *Appl. Phys. Lett.*, vol. 69, no. 17, pp. 2510–2512, Oct. 1996, doi: 10.1063/1.117723.

[41] C. W. Wilson, R. G. Stevie, and F. A. Magee, *Secondary-Ion Mass Spectrometry*. New York, NY, USA: Wiley, 1989.

[42] W. Beyer and F. Einsele, "Hydrogen effusion experiments," in *Advanced Characterization Techniques for Thin Film Solar Cells*, vol. 2. Weinheim, Germany: Wiley-VCH Verlag GmbH & KGaA, 2016, pp. 569–595.

[43] N. Sano, M. Sekiya, M. Hara, A. Kohno, and T. Sameshima, "High quality SiO/sub 2//Si interfaces of poly-crystalline silicon thin film transistors by annealing in wet atmosphere," *IEEE Electron Device Lett.*, vol. 16, no. 5, pp. 157–160, May 1995, doi: 10.1109/55.382225.

[44] Z. Zhang et al., "Improvement of surface passivation of tunnel oxide passivated contact structure by thermal annealing in mixture of water vapor and nitrogen environment," *Sol. RRL*, vol. 3, no. 10, Oct. 2019, Art. no. 1900105, doi: 10.1002/solr.201900105.

[45] S. Reiter et al., "Parasitic absorption in polycrystalline Si-layers for carrier-selective front junctions," *Energy Procedia*, vol. 92, pp. 199–204, Aug. 2016, doi: 10.1016/j.egypro.2016.07.057.

[46] J. I. Pankove, D. E. Carlson, J. E. Berkeyheiser, and R. O. Wance, "Neutralization of shallow acceptor levels in silicon by atomic hydrogen," *Phys. Rev. Lett.*, vol. 51, no. 24, pp. 2224–2225, Dec. 1983, doi: 10.1103/PhysRevLett.51.2224.

[47] N. M. Johnson, C. Herring, and D. J. Chadi, "Interstitial hydrogen and neutralization of shallow-donor impurities in single-crystal silicon," *Phys. Rev. Lett.*, vol. 56, no. 7, pp. 769–772, Feb. 1986, doi: 10.1103/PhysRevLett.56.769.

[48] L.-P. Scheller, M. Weizman, P. Simon, M. Fehr, and N. H. Nickel, "Hydrogen passivation of polycrystalline silicon thin films," *J. Appl. Phys.*, vol. 112, no. 6, Sep. 2012, Art. no. 063711, doi: 10.1063/1.4752268.

[49] P. L. Castro and B. E. Deal, "Low-temperature reduction of fast surface states associated with thermally oxidized silicon," *J. Electrochem. Soc.*, vol. 118, no. 2, 1971, Art. no. 280, doi: 10.1149/1.2408016.

[50] C. Hollemann et al., "Changes in hydrogen concentration and defect state density at the poly-Si/SiO_x/c-Si interface due to firing," *Sol. Energy Mater. Sol. Cells*, vol. 231, 2021, Art. no. 111297, doi: 10.1016/j.solmat.2021.111297.

[51] Z. Rui et al., "On the passivation mechanism of poly-silicon and thin silicon oxide on crystal silicon wafers," *Sol. Energy*, vol. 194, pp. 18–26, Dec. 2019, doi: 10.1016/j.solener.2019.10.064.

[52] M. Lehmann et al., "Analysis of hydrogen distribution and migration in fired passivating contacts (FPC)," *Sol. Energy Mater. Sol. Cells*, vol. 200, 2019, Art. no. 110018, doi: 10.1016/j.solmat.2019.110018.

[53] N. H. Nickel, W. B. Jackson, and J. Walker, "Hydrogen migration in polycrystalline silicon," *Phys. Rev. B*, vol. 53, no. 12, pp. 7750–7761, Mar. 1996, doi: 10.1103/PhysRevB.53.7750.

[54] G. Dingemans, F. Einsele, W. Beyer, M. C. M. Van De Sanden, and W. M. M. Kessels, "Influence of annealing and Al_2O_3 properties on the hydrogen-induced passivation of the Si/SiO_2 interface," *J. Appl. Phys.*, vol. 111, no. 9, 2012, Art. no. 093713, doi: 10.1063/1.4709729.

[55] D. Koushik et al., "Plasma-assisted atomic layer deposition of nickel oxide as hole transport layer for hybrid perovskite solar cells," *J. Mater. Chem. C*, vol. 7, no. 40, pp. 12532–12543, 2019, doi: 10.1039/c9tc04282b.

[56] Y. Elbaz, D. Furman, and M. C. Toroker, "Hydrogen transfer through different crystal phases of nickel oxy/hydroxide," *Phys. Chem. Chem. Phys.*, vol. 20, no. 39, pp. 25169–25178, 2018, doi: 10.1039/C8CP01930D.

[57] T. S. Horányi, "The thermal stability of the β-$Ni(OH)_2$-β-NiOOH system," *Thermochimica Acta*, vol. 137, no. 2, pp. 247–253, Jan. 1989, doi: 10.1016/0040-6031(89)87217-X.

[58] Z.-H. Liang, Y.-J. Zhu, and X.-L. Hu, "β-nickel hydroxide nanosheets and their thermal decomposition to nickel oxide nanosheets," *J. Phys. Chem. B*, vol. 108, no. 11, pp. 3488–3491, Mar. 2004, doi: 10.1021/jp037513n.

[59] G. Parravano, "The reduction of nickel oxide by hydrogen," *J. Amer. Chem. Soc.*, vol. 74, no. 5, pp. 1194–1198, Mar. 1952, doi: 10.1021/ja01125a016.

[60] C. S. Carney, R. E. Chinn, Ö. N. Doğan, and M. C. Gao, "Isothermal decomposition kinetics of nickel (II) hydroxide powder," *J. Alloys Compd.*, vol. 644, pp. 968–974, Sep. 2015, doi: 10.1016/j.jallcom.2015.03.256.

[61] W. Beyer and H. Wagner, "Determination of the hydrogen diffusion coefficient in hydrogenated amorphous silicon from hydrogen effusion experiments," *J. Appl. Phys.*, vol. 53, no. 12, pp. 8745–8750, Dec. 1982, doi: 10.1063/1.330474.

[62] Y. Larionova, V. Mertens, N.-P. Harder, and R. Brendel, "Surface passivation of n-type Czochralski silicon substrates by thermal-SiO_2/plasma-enhanced chemical vapor deposition SiN stacks," *Appl. Phys. Lett.*, vol. 96, no. 3, Jan. 2010, Art. no. 032105, doi: 10.1063/1.3291681.